INORGANIC CHEMISTRY
FRONTIERS

RESEARCH ARTICLE

View Article Online
View Journal | View Issue

Cite this: *Inorg. Chem. Front.*, 2022, **9**, 3436

Two isomeric metal–organic frameworks bearing stilbene moieties for highly volatile iodine uptake†

Jianping Tang,‡[a,b] Shenghua Zhou,‡[a,c] Mengyi Huang,[a,d] Zhenxin Liang,[a] Shaodong Su,[a] Yuehong Wen, *[a,c] Qi-Long Zhu [a,c] and Xintao Wu [a,c]

Efficient, green, and economical removal of radioactive iodine (I_2) has drawn worldwide attention for the safe development of nuclear energy. Metal–organic frameworks (MOFs) have been demonstrated to be potential candidates for I_2 capture. Herein we report the synthesis of two novel isomeric MOFs bearing stilbene moieties for exceptionally high I_2 adsorption. [Cd(hsb-2)(tsbdc)]·0.5DMF (**HSB-W8**) and Cd(hsb-2)(tsbdc) (**HSB-W9**), which exhibit two-dimensional and twofold interpenetrated three-dimensional structures, respectively, have been assembled from hydrogenated Schiff base ligands, hsb-2 (1,2-bis(4′-pyridylmethylamino)-ethane) and trans-stilbene-4,4-dicarboxylate (tsbdc), and $Cd(NO_3)_2$ by the diffusion method. Such isomers arise from the different conformations of hsb-2 ligands controlled by diffusion temperatures. The π-electron-rich stilbene moieties render these Cd-MOFs ideal platforms for I_2 capture. The adsorption capacities of **HSB-W8** and **HSB-W9** in I_2 vapor at room temperature can reach up to 2.32 and 1.92 g g^{-1}, respectively, which are comparable to the best-performing MOF materials reported so far. Furthermore, pseudo-second-order (PSO) kinetic model analysis, Fourier transform infrared (FT-IR) spectroscopy, Raman spectral analysis, density functional theory (DFT) calculations, and control experiments were performed to shed light on host–guest interactions and the iodine adsorption mechanism. This work develops a rational strategy to design and synthesise functional MOF materials for iodine adsorption.

Received 18th April 2022,
Accepted 26th May 2022

DOI: 10.1039/d2qi00835a

rsc.li/frontiers-inorganic

Introduction

With the rise in global population and the rapid economic development of the world, the total world energy demand is set to increase continuously. In the meantime, with the depleting resource of fossil fuels, the search for a low-emission, efficient, and reliable energy source has drawn tremendous attention across the globe.[1] Nuclear energy is often considered a cleaner option for continuous energy production due to its high-density and emission-free nature.[2] During the fission of nuclear fuels, the disposal of radioactive nuclear waste has become a major safety issue in nuclear energy applications.[3,4] Among many volatile radioactive products, release of radioiodine is of great concern, owing to its immediate impact on human health and long-term damage to the environment.[5,6] The applications of activated carbon, zeolites, and other traditional porous materials for iodine capture have been hindered by their relatively low adsorption capacities and low porosities.[7]

Periodic arrangements of metal ions or clusters and bridging organic ligands afford crystalline metal–organic frameworks (MOFs) with tunable and modifiable structures, ultrahigh porosities and surface areas for a large number of applications such as sensing, gas storage, molecular sieving, drug delivery, catalysis, light harvesting and so on.[8–25] Recently, several MOFs have been reported as promising candidates for iodine adsorption.[26–30] Various approaches have been developed to enhance the I_2 adsorption performance of MOF materials;[31] however, rational design and fabrication of MOFs with excellent iodine adsorption still remain big challenges. One effective strategy is to introduce electron-pair donors including pyridine, R_2O, ROH, RNH_2, *etc.*, or conjugated π-electron units into the frameworks to functionalize MOFs, which could form stable halogen bonds or charge-transfer (CT) complexes with I_2, thereby increasing the adsorption capacity.[32–42] It is noteworthy that the adsorption ability is not only concerned with the interaction of I_2 and frameworks,

[a]*State Key Laboratory of Structural Chemistry, Fujian Institute of Research on the Structure of Matter, Chinese Academy of Sciences, Fuzhou 350002, China. E-mail: yhwen@fjirsm.ac.cn*
[b]*College of Chemistry, Fuzhou University, Fuzhou, 350002, China*
[c]*University of Chinese Academy of Sciences, Beijing 100049, China*
[d]*College of Chemistry and Materials Science, Fujian Normal University, Fuzhou 350007, China*

†Electronic supplementary information (ESI) available. CCDC 2051853 and 2132222. For ESI and crystallographic data in CIF or other electronic format see DOI: https://doi.org/10.1039/d2qi00835a

‡These authors contributed equally to this work.

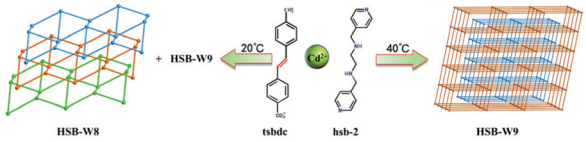

Fig. 1 The structures of hsb-2 and tsbdc, and the schematic illustrations of the diffusion temperature-dependent synthesis of Cd-MOFs **HSB-W8** and **HSB-W9**.

effective sorption sites, and the effect of I_2 (which may form polyiodide anions), but also the surface areas, porosity, pore structures and topology of MOF materials.[31,43,44] Iso-reticular MOFs have provided a good platform to explore I_2 adsorption;[45–47] nonetheless, the utilization of isomeric MOFs with the same active iodine-sorption units, to comparatively study the structure–function relationship and thereafter improve the I_2 uptake capacity, has been rarely reported.

In MOF crystal engineering, polymorphism is a very interesting subject, because such a study is not only important in synthesizing novel materials but also helpful in achieving an elementary understanding of crystal growth.[48–50] MOFs with different topologies can be effectively constructed using the same precursors through controlling the environment. A subtle change of the environment may lead to a drastic change of dimension and topology. For example, in the hydrothermal or solvothermal synthesis of MOFs, temperatures have an unpredictable impact on the structural prediction of the final frameworks.[51–54] But for the diffusion method, the effects of diffusion temperature are usually ignored. In this work, two novel isomeric MOFs, **HSB-W8** and **HSB-W9**, from 1,2-bis(4′-pyridylmethylamino)-ethane (hsb-2), trans-stilbene-4,4-dicarboxylate (tsbdc) and $Cd(NO_3)_2$ were prepared just by adjusting the diffusion temperature (Fig. 1). The integration of π-electron-rich stilbene moieties into frameworks endows these Cd-MOFs with ideal platforms for I_2 capture. **HSB-W8** and **HSB-W9** exhibit abnormally high capacities for iodine adsorption from vapor phases at room temperature. PSO kinetic model analysis, FT-IR spectroscopy, Raman spectral analysis, DFT calculations, and control experiments were performed to shed light on the iodine adsorption mechanism.

Experimental section

Materials and apparatus

All chemicals were purchased commercially and used without further purification except the hsb-2 ligand. The hsb-2 ligand was synthesized according to a previous method.[55–57] Thermal analyses were performed on a NETZSCH STA 449C apparatus from 20 to 1000 °C at a heating rate of 10 °C min^{-1} under nitrogen flow. Elemental analyses (C, H, and N) were performed using a Vario MICRO CHNOS elemental analyzer. Fourier-transform infrared spectra were recorded in the range of 4000–400 cm^{-1} on a PerkinElmer Spectrum Two FT-IR spectrometer. PXRD data were recorded on a DMAX-2500 diffractometer with Cu-Ka radiation.

Crystal structure determination

The structure was solved by the SHELXL-2017 and OLEX2 program package.[58,59] All the non-hydrogen atoms were refined anisotropically, and the hydrogen atoms attached to carbon were located at their ideal positions. The details of the crystal data are presented in Tables S1 and S2 (ESI†).

The CCDC numbers are 2051853 and 2132222 for **HSB-W8** and **HSB-W9**.†

Synthesis of the HSB-W8 MOF. Method 1: A solution of $Cd(NO_3)_2{\cdot}4H_2O$ (0.1 mmol) in H_2O/EtOH (12 mL, 7 : 5) was layered over a solution of hsb-2 (0.1 mmol) and tsbdc (0.1 mmol) in H_2O/DMF (12 mL, 2 : 1) at 20 °C. Colorless crystals of **HSB-W8** (16 mg) were isolated after two months in 23.6% yield based on the hsb-2 ligand. Anal. calcd for [Cd(hsb-2)(tsbdc)]·$2H_2O$·0.5DMF: C 54.55%, H 5.16%, N 9.09%; found: C 54.78%, H 5.12%, N 9.51%. IR (KBr): ν = 3649(w), 3519(vw), 3459(vw), 3303(vw), 3060(w), 2953(m), 2919(m), 2844(w), 2819(vw), 1934(vw), 1593(vs), 1541(vs), 1379(vs), 1300(m), 1230(m), 1175(m), 1107(m), 1072(m), 1012(s), 954(m), 862(m), 788(vs), 851(vw), 711(s), 621(m), 551(w), 519(m) cm^{-1}.

Method 2: A solution of tsbdc (0.2 mmol) and hsb-2 (0.3 mmol) in H_2O (12 mL) was added to $Cd(NO_3)_2{\cdot}4H_2O$ (0.2 mmol) in H_2O (12 mL) under ultrasonic irradiation. After 20 min, the milky colloidal suspension was centrifugated at 10 000 rpm for 5 min to obtain the sediments, and then they were washed with DMF and EtOH. Finally, 85 mg of **HSB-W8** were obtained by drying, corresponding to 63% yield based on tsbdc.

Synthesis of the HSB-W9 MOF. A solution of $Cd(NO_3)_2{\cdot}4H_2O$ (0.1 mmol) in H_2O/EtOH (12 mL, 7 : 5) was layered over a solution of hsb-2 (0.1 mmol) and tsbdc (0.1 mmol) in H_2O/DMF (12 mL, 2 : 1) at 40 °C. Colorless crystals of **HSB-W9** (22.2 mg) were isolated after two months in 32.8% yield based on the hsb-2 ligand. Anal. calcd for [Cd(hsb-2)(tsbdc)]·$4H_2O$: C 51.99%, H 5.24%, N 8.08%; found: C 52.23%, H 4.88%, N 8.12%. IR (KBr): ν = 3428(vs), 3227(vs), 3059(s), 2944(s), 2851(m), 1591(vs), 1542(vs), 1382(vs), 1305(m), 1226(w), 1180(m), 1141(vw), 1109(vw), 1011(w), 961(w), 864(m), 790(s), 707(m), 635(vw), 537(vw), 496(vw), 421(vw) cm^{-1}.

Iodine adsorption and release. An open sample vial with 30 mg of Cd-MOF was placed in another sealed weighing bottle equipped with excess iodine and maintained at 25 °C under ambient atmospheric pressure, and then weighed after specified time intervals. The iodine adsorption capacity was expressed by the following equation:

$$\alpha = \frac{m_2 - m_1}{m_1}$$

where α is the amount of iodine adsorption capacity (wt%), and m_1 and m_2 are the masses of the samples before and after iodine adsorption (mg), respectively.

After iodine adsorption, the sample was exposed to air at room temperature, and the stability of bound iodine was investigated through measuring the change of the Cd-MOF weight.

A 5 mg sample of the **HSB-W8** or **HSB-W9** adsorbent (denoted as I_2@**HSB-W8** and I_2@**HSB-W9**, respectively) was subjected to desorption in methanol (20 ml) for different contact times, ranging from 0 to 400 min at 25 °C. At a certain time, I_2@**HSB-W8** and I_2@**HSB-W9** were filtered off, and the I_2 concentration in methanol solution was determined by UV-vis spectrophotometry.

Results and discussion

Synthesis and crystal structure

The various conformations of the hydrogenated Schiff base ligand hsb-2 make the synthesis of isomeric MOFs possible and the introduction of tsbdc with the π-electron-rich stilbene unit is expected to realize the efficient adsorption of iodine.[43] Fortunately, the bulk single crystals of **HSB-W8**, [Cd(hsb-2)(tsbdc)]·0.5DMF, and **HSB-W9**, Cd(hsb-2)(tsbdc), were synthesized through the slow diffusion technique using hsb-2, tsbdc, and $Cd(NO_3)_2$ at different temperatures. When the solution was kept standing for several days at 20 °C, crystals of **HSB-W9** with a block shape gradually appeared on the lower tube wall containing the mixed ligand. Needlelike crystals of **HSB-W8** were grown just at the interface of the two solutions within one week. As time goes on, **HSB-W8** gradually grew into dendritic crystals. The yields of **HSB-W8** and **HSB-W9** are up to 23.6% and 24.4%, respectively. Notably, only one type of crystal, **HSB-W9**, was grown at 40 °C. In addition, uniform **HSB-W8** can also be obtained rapidly and in large quantities with a yield up to 63% by directly mixing the precursors under ultrasonic conditions (Fig. S1, ESI†).

The single-crystal X-ray crystallographic analysis reveals the structure and difference of the obtained two Cd-MOFs. **HSB-W8** and **HSB-W9** crystallize in the triclinic space group $P\bar{1}$ and monoclinic space group $C2/c$, respectively (Table S1, ESI†). All the Cd(II) centers adopt a distorted octahedron $[CdN_4O_2]$ coordination geometry, which is formed by two secondary amine nitrogen atoms from one hsb-2 and two pyridine nitrogen atoms from another hsb-2 composing the equatorial plane, and two oxygen atoms from two tsbdc ligands at the apical positions (Fig. 2a). In the structure of **HSB-W8**, the bond lengths of Cd–N vary from 2.383(5) to 2.427(5) Å, and the two Cd–O distances are 2.258(4) and 2.262(4) Å, respectively, while the bond angles around Cd(II) ions are in the range of 77.07(16)°–175.54 (16)° (Table S2, ESI†). In **HSB-W9**, the bond lengths of Cd–N are 2.337(7)–2.377(8) Å, and both Cd–O distances are 2.287(7) Å, respectively, while the bond angles around Cd(II) ions are in the range of 76.4(4)°–177.0 (4)° (Table S3, ESI†). All the hsb-2 ligands in **HSB-W8** display an unusual "C" shape, which are coordinated with Cd(II) ions to form infinite $[Cd(hsb\text{-}2)]_n$ double-chains (Fig. 2b). These double-chains are further bridged by the tsbdc ligands through sharing the Cd(II) ions, resulting in a 2D 4^4-sql layered structure (Fig. 2c). Adjacent layers in **HSB-W8** are stacked in an ABC manner through weak intermolecular interactions (Fig. 2d and e). Differently, "W"-shaped hsb-2 ligands in

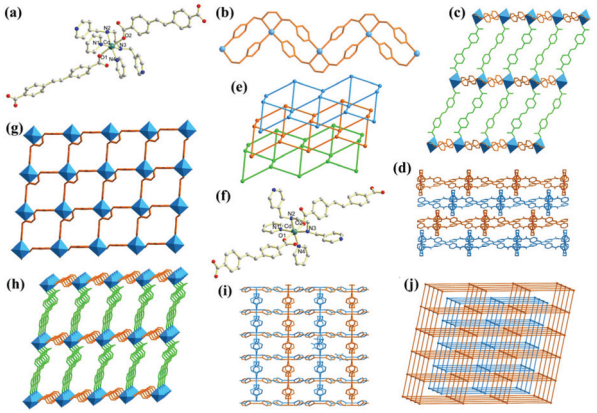

Fig. 2 Views of the coordination environments of the Cd(II) ion in **HSB-W8** (a) and **HSB-W9** (f) (hydrogen atoms and solvent molecules have been omitted for clarity). (b) The 1D double-zigzag sub-chain in **HSB-W8**. (c) A 2D layer of **HSB-W8**. (d) The stacking manner of **HSB-W8** layers. (e) Topological presentation of **HSB-W8**. (g) A 2D layer of **HSB-W9**. (h) A part of the 3D structure of **HSB-W9**. (i) The twofold interpenetrated structure of **HSB-W9**. (j) Topological presentation of **HSB-W9**.

HSB-W9 link the Cd(II) centers to compose a 2D network with rhombic windows. Different layers are further connected by tsbdc to form a 3D pillar-layered framework with large windows along the *a* axis (Fig. 2f, g and h). To minimize the large void cavities and stabilize the framework, two identical 3D frameworks are interspersed with each other to form the final twofold interpenetrated structure of **HSB-W9** (Fig. 2j). Although interpenetration occurs, there still exist 1D small channels along the *a* axis, with aperture sizes of about 0.8 nm × 0.9 nm (Fig. 2i). The accessible void calculated by PLATON/SOLV analysis is estimated to be 25.6% without consideration of the solvent molecules. Meanwhile, **HSB-W8** has 1D channels with dimensions of approximately 0.6 nm × 0.7 nm (Fig. 2d), and an accessible void of 23.1%.

HSB-W8 and **HSB-W9** are two MOF isomers, which contain the same building components but display different supramolecular structures. The topological difference is ascribed to the flexibility of the hsb-2 ligand. During the self-assembly process, the conformations of hsb-2 can be controlled by the diffusion temperature. At lower temperatures, hsb-2 can exhibit both the "C" and "W" conformations, while at higher temperatures hsb-2 tends to adopt only the "W" shape, when coordinating with Cd(II) ions, which leads to formation of 1D double-chains and 2D layers of $[Cd(hsb\text{-}2)]_n$ subunits, respectively. These double-chains and layers are further linked by tsbdc pillar ligands to afford a 2D layered network of **HSB-W8** and 3D pillar-layered frameworks of **HSB-W9**. Therefore, it is a rational strategy to prepare MOF isomers through tuning the diffusion temperature to change the conformation of ligands.[60]

Iodine capture performance

The stilbene moiety of tsbdc is expected to become active sites for I_2 adsorption, leading to the Cd-MOFs as good I_2 adsorbent

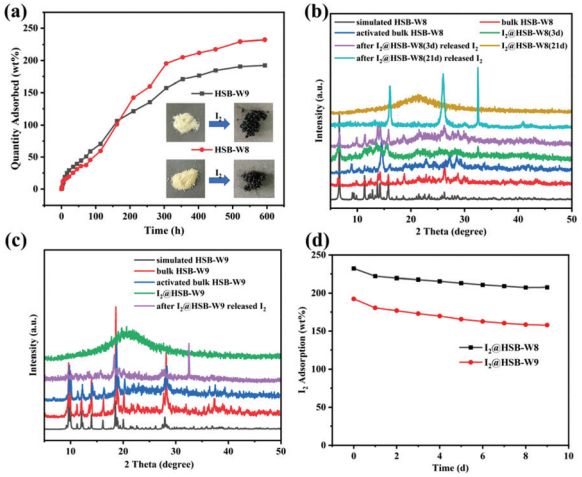

Fig. 3 (a) Adsorption curves and the color evolution of the Cd-MOFs at 25 °C in iodine vapor. (b) The PXRD patterns of **HSB-W8** at different stages. (c) The PXRD patterns of **HSB-W9** at different stages. (d) Stability of iodine-loaded Cd-MOFs at room temperature.

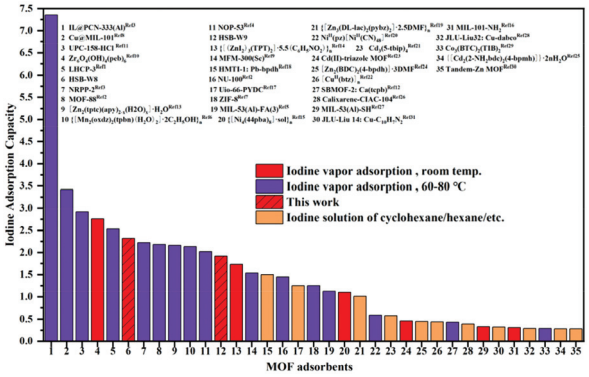

Fig. 4 Iodine adsorption capacities of different MOF adsorbents (the references are arranged in the ESI†).

candidates. The adsorption capacities at different contact times for a Cd-MOF at 25 °C were monitored to investigate their capture performance toward iodine. The photographs of the Cd-MOF before and after iodine adsorption are shown in Fig. 3a. It can be seen that these adsorbents displayed a color change from white to black with the loaded iodine. The adsorption rate increased rapidly within the initial 16 h of adsorption and adsorption saturation was achieved at 21 d. In the early stages of I_2 adsorption, **HSB-W8** and **HSB-W9** displayed closely matched adsorption curves. For **HSB-W8**, the iodine adsorption rate increased significantly after 3.5 d, which may be due to the augmenting of interlamellar spacing caused by the accumulation of a large amount of I_2 between **HSB-W8** layers. The iodine-loaded **HSB-W8** was soaked in methanol to release the adsorbed iodine after 3 d of adsorption, and the PXRD pattern remained basically unchanged. In contrast, the PXRD pattern of **HSB-W8** changed significantly after 21 days of adsorption, indicating the collapse of the MOF framework (Fig. 3b). The diffraction peaks of **HSB-W9** became very weak after iodine adsorption. After releasing I_2, the XRD peaks recovered, but the relative intensities of some peaks weakened slightly as compared to those of pristine **HSB-W9** (Fig. 3c), which might be attributed to the residual I_2 in cavities consequently leading to the diminished X-ray contrast between the porous framework and pore channels.[61] The equilibrium adsorption capacities of **HSB-W8** and **HSB-W9** for iodine could reach up to 2.32 and 1.92 g g^{-1}, respectively.

To understand iodine adsorption kinetics on the Cd-MOF, pseudo-second-order (PSO) kinetic models[62] were applied to fit the experimental data. The good fitting results (R^2 > 0.98) obtained for the **HSB-W8** and **HSB-W9** samples (Fig. S2 and S3†) indicate a strong chemical interaction between iodine and the framework.[63] The desorption behavior of iodine in the adsorbent at room temperature is an important index for the stability of bound iodine; therefore, the two iodine-loaded Cd-MOFs were placed in air at room temperature. As the change of adsorption capacity shows in Fig. 3d, in the initial day, the adsorption capacity rapidly decreased and then slowed, and maintained a mainly constant level (>207 wt% for **HSB-W8** and >158 wt% for **HSB-W9**) after 8 days with a high iodine load, which indicated that the bound iodine in Cd-MOFs was relatively stable. We have summarized results of more than thirty MOF adsorbents for iodine capture in Fig. 4. It is worth noting that both Cd-MOF isomers have outstanding iodine adsorption capacity at room temperature.

As a potential iodine absorber, the assessment of renewability for Cd-MOFs is necessary before practical applications. Therefore, a desorption experiment was performed in methanol at room temperature. With an extension of the desorption time, the color of the solution changed from light to dark (Fig. S4, ESI†). As shown in Fig. S5 and Table S4, ESI,† the release of iodine is in equilibrium with a recovery rate of more than 93% after 400 min. Because **HSB-W8** and **HSB-W9** have a high affinity towards iodine, there was still some iodine residue after elution with methanol several times; therefore, the recirculation performance of the two Cd-MOFs is greatly limited. After the first reuse, there were only 15% and 29% weight ratio gains for **HSB-W8** and **HSB-W9**. Considering the green and facile synthesis path and the high adsorption capacity of iodine at room temperature, these two Cd-MOFs can also be used as potential disposable adsorbents for iodine.

Adsorption mechanism

The interaction between Cd-MOFs and iodine was studied by thermogravimetric (TG) analysis, FT-IR spectroscopy, Raman spectroscopy, density functional theory (DFT) calculations, and controlled experiments. The TG curves of I_2@**HSB-W8** and I_2@**HSB-W9** exhibit a sharp decrease in the range of 30–200 °C, which may be due to the release of I_2 from the surface and pores of the frameworks. The twofold interpenetrated structure of **HSB-W9** made it difficult for some I_2 to escape. It is, therefore, plausible that the decreasing rate of the TG curve slowed down obviously before the collapse of the skeleton in the range of 200–280 °C. Additionally, the volatiliz-

ation of I_2 with a strong interaction with Cd-MOFs may lead to the TG curve of I_2@Cd-MOFs being significantly different from those of the isomeric Cd-MOFs (Fig. S6 and S7, ESI†). The FT-IR spectra of **HSB-W9** after iodine adsorption (Fig. S8, ESI†) show that the characteristic peaks of N–H (3446 cm^{-1}) and C–N (1141 cm^{-1}) stretchings in the secondary amine in I_2@**HSB-W9** changed compared to those in pristine **HSB-W9**. Meanwhile, the characteristic peaks of C=C stretching (1664 cm^{-1}), C–H in-plane bending (1257 cm^{-1}) and C–H out-of-plane bending (974 cm^{-1}) have obviously changed after iodine adsorption. There is a similar situation in **HSB-W8** (Fig. S9, ESI†). This indicated that both the secondary amine and stilbene may be active sites for iodine adsorption. To further reveal the adsorption mechanisms of **HSB-W8** and **HSB-W9**, DFT calculations were carried out to investigate the interaction between MOF adsorbents and I_2 molecules. A representative section of **HSB-W8** and **HSB-W9** that includes their asymmetric units was selected for calculations. As shown in Fig. 5, the distances between I_2 and the carbon–carbon double bond of stilbene in **HSB-W8** and **HSB-W9** are 3.282 Å and 3.954 Å, respectively, which are much shorter than the distances between the I_2 and N atoms of the secondary amine in hsb-2 (4.712 Å and 4.656 Å). From Table S5, ESI,† it is obvious that the calculated adsorption energy of I_2 molecules interacting with the stilbene moieties is also higher than that of I_2 and secondary amines. These calculation results illustrated that the stilbene moieties play an important role for the high I_2 uptake properties in these two Cd-MOFs. This was also verified by the parallel experiments of the iso-reticular **HSB-W7** MOF (Fig. S10, ESI†).[64] The structure of **HSB-W7** is similar to that of **HSB-W8** except that the tsbdc ligands were replaced by 2-hydroxybenzate. In the absence of stilbene units, **HSB-W7** exhibits poor I_2 uptake capacity. According to the Raman spectra (Fig. S11 and S12, ESI†), two new peaks located at low wavenumbers of 107 and 168 cm^{-1} appeared after iodine adsorption, which correspond to the symmetric stretching of $I_3^-$and I_5^-, respectively,[65–67] whereas the peak position of I_2 was observed at 183 cm^{-1}.[68] The above analyses implied that the high iodine adsorption capacity of Cd-MOFs was mainly attributed to electron transfer between the π-electron-rich stilbene and iodine, alluding to a chemisorption process, and the main chemical form of iodine was polyiodide anions from a charge transfer complex (CT) process.[69,70] Besides the active sites, the topological structure also affects the iodine adsorption properties. In this system, at the early stage of the I_2 uptake process, the adsorption abilities of **HSB-W8** and **HSB-W9** are comparable, which can be attributed to their same active sites and similarly accessible voids; while in the later stage, the adsorption capacity of **HSB-W8** was more predominant, owing to the flexible interlamellar spacing feature of layered MOFs. With the increase of adsorbed iodine, the interlamellar spacing of **HSB-W8** becomes larger and larger, which finally results in the destruction of its crystalline nature. **HSB-W9** has a twofold interpenetrated 3D pillar-layered structure, the regular and rigid porous structure of which can keep the framework undamaged during the whole iodine absorption process.

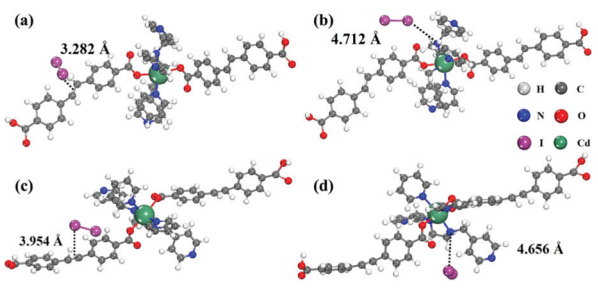

Fig. 5 (a and b) Optimized geometries of **HSB-W8** interacting with I_2 molecules and (c and d) optimized geometries of **HSB-W9** interacting with I_2 molecules.

Conclusions

In summary, two novel Cd-MOF isomers, **HSB-W8** and **HSB-W9**, have been prepared from the same mixed ligands of hydrogenated Schiff base, hsb-2, and dicarboxylate, tsbdc, at different diffusion temperatures. **HSB-W8** is a 2D layer network, while **HSB-W9** shows a twofold interpenetrated 3D pillar-layered framework, the structural difference of which is ascribed to the flexibility of the hsb-2 ligand. **HSB-W8** and **HSB-W9** exhibit superior I_2 adsorption abilities at room temperature, with maximum adsorption capacities of 2.32 and 1.92 g g^{-1} under I_2 vapor conditions, respectively. The kinetics were well fitted by the PSO kinetic model, suggesting a chemisorption process. The π-electron-rich stilbene moieties in tsbdc play important roles for the high iodine uptake. **HSB-W8** and **HSB-W9** exhibit different I_2 adsorption capacities and processes, which are mainly caused by their structural differences. The adsorption mechanism was studied according to TG analysis, FT-IR spectra, Raman spectra, DFT calculations, and control experiments. This work establishes stilbene-functionalized MOFs as promising candidates for highly radioactive iodine uptake, and enriches the study of polymorphism in MOFs. Further research will be focused on the rational design and synthesis of more efficient I_2 sorbents based on π-electron-rich MOFs, intending to shorten the adsorption time and improve recyclability.

Author contributions

J. P. Tang and Y. H. Wen designed and carried out the experiments. S. H. Zhou carried out the DFT calculations. M. Y. Huang and Z. X. Liang performed the XRD and SCXRD measurements. S. D. Su offered help in the single crystal growth and test. X. T. Wu provided discussion on the assembly strategy. J. P. Tang and Y. H. Wen prepared the manuscript. J. P. Tang, Y. H. Wen and Q.-L. Zhu conceived the experiments, analysed the results, and revised the manuscript. All the authors have approved the final version of the manuscript.

Conflicts of interest

The authors declare no conflict of interest.

Acknowledgements

This work was financially supported by the National Natural Science Foundation of China (NSFC) (21901246), the Strategic Priority Research Program of CAS (XDB20010200), and the Natural Science Foundation of Fujian Province (2019J01126).

References

1 S. Chu and A. Majumdar, Opportunities and challenges for a sustainable energy future, *Nature*, 2012, **488**, 294–303.
2 D. Banerjee, A. J. Cairns, J. Liu, R. K. Motkuri, S. K. Nune, C. A. Fernandez, R. Krishna, D. M. Strachan and P. K. Thallapally, Potential of Metal-Organic Frameworks for Separation of Xenon and Krypton, *Acc. Chem. Res.*, 2015, **48**, 211–219.
3 Y. Zhao, Emerging Applications of Metal–Organic Frameworks and Covalent Organic Frameworks, *Chem. Mater.*, 2016, **28**, 8079–8081.
4 J. Liu, Y. Wei and Y. Zhao, Trace Carbon Dioxide Capture by Metal–Organic Frameworks, *ACS Sustainable Chem. Eng.*, 2019, **7**, 82–93.
5 Y. H. Abdelmoaty, T. D. Tessema, F. A. Choudhury, O. M. El-Kadri and H. M. El-Kaderi, Nitrogen-rich porous polymers for carbon dioxide and iodine sequestration for environmental remediation, *ACS Appl. Mater. Interfaces*, 2018, **10**, 16049–16058.
6 M. Xu, T. Wang, L. Zhou and D. Hua, Fluorescent conjugated mesoporous polymers with N, N-diethylpropylamine for the efficient capture and real-time detection of volatile iodine, *J. Mater. Chem. A*, 2020, **8**, 1966–1974.
7 J. Huve, A. Ryzhikov, H. Nouali, V. Lalia, G. Augé and T. J. Daou, Porous Sorbents for the Capture of Radioactive Iodine Compounds: A Review, *RSC Adv.*, 2018, **8**, 29248–29273.
8 O. M. Yaghi, M. O'Keeffe, N. W. Ockwig, H. K. Chae, M. Eddaoudi and J. Kim, Reticular synthesis and the design of new materials, *Nature*, 2003, **423**, 705–714.
9 Y. Liu, W. Xuan and Y. Cui, Engineering homochiral metal-organic frameworks for heterogeneous asymmetric catalysis and enantioselective separation, *Adv. Mater.*, 2010, **22**, 4112–4135.
10 J.-P. Zhang, Y.-B. Zhang, J.-B. Lin and X.-M. Chen, Metal Azolate Frameworks: From Crystal Engineering to Functional Materials, *Chem. Rev.*, 2012, **112**, 1001–1033.
11 A. Kirchon, L. Feng, H. F. Drake, E. A. Joseph and H.-C. Zhou, From fundamentals to applications: a toolbox for robust and multifunctional MOF materials, *Chem. Soc. Rev.*, 2018, **47**, 8611–8638.
12 Y. H. Wen, J. Zhang, Q. Xu, X. T. Wu and Q. L. Zhu, Pore surface engineering of metal-organic frameworks for heterogeneous catalysis, *Coord. Chem. Rev.*, 2018, **376**, 248–276.
13 L. Zhu, X.-Q. Liu, H.-L. Jiang and L.-B. Sun, Metal-Organic Frameworks for Heterogeneous Basic Catalysis, *Chem. Rev.*, 2017, **117**, 8129–8176.
14 L. E. Kreno, K. Leong, O. K. Farha, M. Allendorf, R. P. Van Duyne and J. T. Hupp, Metal-Organic Framework Materials as Chemical Sensors, *Chem. Rev.*, 2012, **112**, 1105–1125.
15 Y. J. Cui, Y. F. Yue, G. D. Qian and B. L. Chen, Luminescent Functional Metal-Organic Frameworks, *Chem. Rev.*, 2012, **112**, 1126–1162.
16 H. Y. Li, S. N. Zhao, S. Q. Zang and J. Li, Functional metal-organic frameworks as effective sensors of gases and volatile compounds, *Chem. Soc. Rev.*, 2020, **49**, 6364–6401.
17 T. R. Cook, Y.-R. Zheng and P. J. Stang, Metal-Organic Frameworks and Self-Assembled Supramolecular Coordination Complexes: Comparing and Contrasting the Design, Synthesis, and Functionality of Metal-Organic Materials, *Chem. Rev.*, 2013, **113**, 734–777.
18 X. Zhao, Y. Wang, D.-S. Li, X. Bu and P. Feng, Metal-organic frameworks for separation, *Adv. Mater.*, 2018, **30**, 1705189.
19 M. Pan, W.-M. Liao, S.-Y. Yin, S.-S. Sun and C.-Y. Su, Single-phase white-light-emitting and photoluminescent color-tuning coordination assemblies, *Chem. Rev.*, 2018, **118**, 8889–8935.
20 M. Dinca and J. R. Long, Introduction: Porous Framework Chemistry, *Chem. Rev.*, 2020, **120**, 8037–8038.
21 G. R. Cai, P. Yan, L. L. Zhang, H.-C. Zhou and H.-L. Jiang, Metal-Organic Framework-Based Hierarchically Porous Materials: Synthesis and Applications, *Chem. Rev.*, 2021, **121**, 12278–12326.
22 X. Wang, P. C. Lan and S. Ma, Metal-Organic Frameworks for Enzyme Immobilization: Beyond Host Matrix Materials, *ACS Cent. Sci.*, 2020, **6**, 1497–1506.
23 Y. T. Qian, F. F. Zhang and H. Pang, A Review of MOFs and Their Composites-Based Photocatalysts: Synthesis and Applications, *Adv. Funct. Mater.*, 2021, **31**, 2104231.
24 Y. Jiao, Y. Zuo, H. Yang, X. Gao and C. Y. Duan, Photoresponse within dye-incorporated metal-organic architectures, *Coord. Chem. Rev.*, 2021, **430**, 213648.
25 Z. Chang, D.-H. Yang, J. Xu, T.-L. Hu and X.-H. Bu, Flexible Metal–Organic Frameworks: Recent Advances and Potential Applications, *Adv. Mater.*, 2015, **27**, 5432–5441.
26 Z. Yin, Q. X. Wang and M. H. Zeng, Iodine release and recovery, influence of polyiodide anions on electrical conductivity and nonlinear optical activity in an interdigitated and interpenetrated bipillared-bilayer metal–organic framework, *J. Am. Chem. Soc.*, 2012, **134**, 4857–4863.
27 X. L. Hu, C. Y. Sun, C. Qin, X. L. Wang, H. N. Wang, E. L. Zhou, W. E. Li and Z. M. Su, Iodine-templated assembly of unprecedented 3d–4f metal–organic frameworks as photocatalysts for hydrogen generation, *Chem. Commun.*, 2013, **49**, 3564–3566.

28 T. He, X. Xu, B. Ni, H. Lin, C. Li, W. Hu and X. Wang, Metal–Organic Framework Based Microcapsules, *Angew. Chem., Int. Ed.*, 2018, **57**, 10148–10152.
29 Y.-L. Wang, X.-Y. Li, S.-D. Han, J. Pan and Z.-Z. Xue, Cu_2I_2-Based Coordination Framework as the Selective Sensor for Ag+ and the Effective Adsorbent for I_2, *Cryst. Growth Des.*, 2022, **22**, 3719–3726.
30 L. J. Small, R. C. Hill, J. L. Krumhansl, M. E. Schindelholz, Z. Chen, K. W. Chapman, X. Zhang, S. Yang, M. Schroder and T. M. Nenoff, Reversible MOF-Based Sensors for the Electrical Detection of Iodine Gas, *ACS Appl. Mater. Interfaces*, 2019, **11**, 27982–27988.
31 X. R. Zhang, J. Maddock, T. M. Nenoff, M. A. Denecke, S. H. Yang and M. Schröder, Adsorption of iodine in metal–organic framework materials, *Chem. Soc. Rev.*, 2022, **51**, 3243–3262.
32 Y. R. Lee, X. H. Do, K. Y. Cho, K. Jeong and K.-Y. Baek, Amine-Functionalized Zeolitic Imidazolate Framework-8 (ZIF-8) Nanocrystals for Adsorption of Radioactive Iodine, *ACS Appl. Nano Mater.*, 2020, **3**, 9852–9861.
33 R. X. Yao, X. Cui, X. X. Jia, F. Q. Zhang and X. M. Zhang, A Luminescent Zinc(II) Metal-Organic Framework (MOF) with Conjugated pi-Electron Ligand for High Iodine Capture and Nitro-Explosive Detection, *Inorg. Chem.*, 2016, **55**, 9270–9275.
34 M.-H. Zeng, Q.-X. Wang, Y.-X. Tan, S. Hu, H.-X. Zhao, L.-S. Long and M. Kurmoo, Rigid Pillars and Double Walls in a Porous Metal-Organic Framework: Single-Crystal to Single-Crystal, Controlled Uptake and Release of Iodine and Electrical Conductivity, *J. Am. Chem. Soc.*, 2010, **132**, 2561–2563.
35 M.-H. Zeng, Z. Yin, Y.-X. Tan, W.-X. Zhang, Y.-P. He and M. Kurmoo, Nanoporous Cobalt(II) MOF Exhibiting Four Magnetic Ground States and Changes in Gas Sorption upon Post-Synthetic Modification, *J. Am. Chem. Soc.*, 2014, **136**, 4680–4688.
36 S. Wang, Q. Hu, Y. Liu, X. Meng, Y. Ye, X. Liu, X. Song and Z. Liang, Multifunctional conjugated microporous polymers with pyridine unit for efficient iodine sequestration, exceptional tetracycline sensing and removal, *J. Hazard. Mater.*, 2020, **387**, 121949.
37 T. Geng, Z. Zhu, W. Zhang and Y. Wang, A nitrogen-rich fluorescent conjugated microporous polymer with triazine and triphenylamine units for high iodine capture and nitro aromatic compound detection, *J. Mater. Chem. A*, 2017, **5**, 7612–7617.
38 Y. Chen, H. Sun, R. Yang, T. Wang, C. Pei, Z. Xiang, Z. Zhu, W. Liang, A. Li and W. Deng, Synthesis of conjugated microporous polymer nanotubes with large surface areas as absorbents for iodine and CO_2 uptake, *J. Mater. Chem. A*, 2015, **3**, 87–91.
39 J. T. Hughes, D. F. Sava, T. M. Nenoff and A. Navrotsky, Thermochemical Evidence for Strong Iodine Chemisorption by ZIF-8, *J. Am. Chem. Soc.*, 2013, **135**, 16256–16259.
40 L. Wang, T. Li, X. Dong, M. Pang, S. Xiao and W. Zhang, Thiophene-based MOFs for iodine capture: Effect of pore structures and interaction mechanism, *Chem. Eng. J.*, 2021, **425**, 130578.
41 B. Guo, F. Li, C. Wang, L. Zhang and D. Sun, A rare (3,12)-connected zirconium metal–organic framework with efficient iodine adsorption capacity and pH sensing, *J. Mater. Chem. A*, 2019, **7**, 13173–13179.
42 Z. Akimbekov, A. D. Katsenis, G.P Nagabhushana, G. Ayoub, M. Arhangelskis, A. J. Morris, T. Friščić and A. Navrotsky, Experimental and theoretical evaluation of the stability of true MOF polymorphs explains their mechanochemical interconversions, *J. Am. Chem. Soc.*, 2017, **23**, 7952–7957.
43 C. Falaise, C. Volkringer, J. Facqueur, T. Bousquet, L. Gasnot and T. Loiseau, Capture of iodine in highly stable metal-organic frameworks: A systematic study, *Chem. Commun.*, 2013, **49**, 10320–10322.
44 W. Xie, D. Cui, S.-R. Zhang, Y.-H. Xu and D.-L. Jiang, Iodine capture in porous organic polymers and metal–organic frameworks materials, *Mater. Horiz.*, 2019, **6**, 1571–1595.
45 R. J. Marshall, S. L. Griffin, C. Wilson and R. S. Forgan, Stereoselective Halogenation of Integral Unsaturated C-C Bonds in Chemically and Mechanically Robust Zr and Hf MOFs, *Chem. – Eur. J.*, 2016, **22**, 4870–4877.
46 Z.-J. Li, Y. Ju, B. Yu, X. Wu, H. Lu, Y. Li, J. Zhou, X. Guo, Z.-H. Zhang, J. Lin, J.-Q. Wang and S. Wang, Modulated synthesis and isoreticular expansion of Th-MOFs with record high pore volume and surface area for iodine adsorption, *Chem. Commun.*, 2020, **56**, 6715–6718.
47 P. Chen, X. He, M. Pang, X. Dong, S. Zhao and W. Zhang, Iodine Capture Using Zr-Based Metal-Organic Frameworks (Zr-MOFs): Adsorption Performance and Mechanism, *ACS Appl. Mater. Interfaces*, 2020, **12**, 20429–20439.
48 B. Karadeniz, D. Zilic, I. Huskic, L. S. Germann, A. M. Fidelli, S. Muratovic, I. Loncaric, M. Etter, R. E. Dinnebier, D. Barisic, N. Cindro, T. Islamoglu, O. K. Farha, T. Friscic and K. Uzarevic, Controlling the Polymorphism and Topology Transformation in Porphyrinic Zirconium Metal-Organic Frameworks via Mechanochemistry, *J. Am. Chem. Soc.*, 2019, **141**, 19214–19220.
49 T. A. Makal, A. A. Yakovenko and H.-C. Zhou, Isomerism in Metal-Organic Frameworks: "Framework Isomers", *J. Phys. Chem. Lett.*, 2011, **2**, 1682–1689.
50 J.-P. Zhang, X.-C. Huang and X.-M. Chen, Supramolecular isomerism in coordination polymers, *Chem. Soc. Rev.*, 2009, **38**, 2385–2396.
51 G.-X. Liu, H. Xu, H. Zhou, S. Nishihara and X.-M. Ren, Temperature-induced assembly of MOF polymorphs: Syntheses, structures and physical properties, *CrystEngComm*, 2012, **14**, 1856–1864.
52 P. Mahata, A. Sundaresan and S. Natarajan, The role of temperature on the structure and dimensionality of MOFs: an illustrative study of the formation of manganese oxy-bis (benzoate) structures, *Chem. Commun.*, 2007, **43**, 4471–4473.
53 K. Sheng, L.-M. Fan, X.-F. Tian, R. K. Gupta, L. Gao, C.-H. Tung and D. Sun, Temperature-induced Sn(II) supra-

molecular isomeric frameworks as promising heterogeneous catalysts for cyanosilylation of aldehydes, *Sci. China: Chem.*, 2020, **63**, 182–186.

54 H. Ju, Y. Habata and S. S. Lee, Temperature-Dependent Supramolecular Isomeric Zn(II)-Metal–Organic Frameworks and Their Guest Exchange, *Cryst. Growth Des.*, 2020, **20**, 4640–4648.

55 B.-L. Fei, W.-Y. Sun, K.-B. Yu and W.-X. Tang, Construction of co-ordination networks of 1,6-bis (4′-pyridyl)-2,5-diazahexane with silver(I) and copper(I). Structural diversity through change in metal ions and counter ions, *J. Chem. Soc., Dalton Trans.*, 2000, **5**, 805–811.

56 Y. H. Wen, T. L. Sheng, S. M. Hu, Y. L. Wang, C. H. Tan, X. Ma, Z. Z. Xue, Y. Wang and X. T. Wu, Effect of anions on the self-assembly of Zn(II) with a hydrogenated Schiff base ligand: structural diversity and photoluminescent properties, *CrystEngComm*, 2013, **15**, 2714–2721.

57 Y. H. Wen, T. L. Sheng, C. Zhuo, X. Q. Zhu, S. M. Hu, W. H. Cao, H. R. Li, H. Zhang and X. T. Wu, 1D to 3D and Chiral to Noncentrosymmetric Metal-Organic Complexes Controlled by the Amount of DEF Solvent: Photoluminescent and NLO Properties, *Inorg. Chem.*, 2016, **55**, 4199–4205.

58 O. V. Dolomanov, L. J. Bourhis, R. J. Gildea, J. A. K. Howard and H. Puschmann, OLEX2: a complete structure solution, refinement and analysis program, *J. Appl. Crystallogr.*, 2009, **42**, 339–341.

59 G. M. Sheldrick, Crystal structure refinement with SHELXL, *Acta Crystallogr., Sect. C: Struct. Chem.*, 2015, **71**, 3–8.

60 N. Li, R. Feng, J. Zhu, Z. Chang and X.-H. Bu, Conformation versatility of ligands in coordination polymers: From structural diversity to properties and applications, *Coord. Chem. Rev.*, 2018, **375**, 558–586.

61 J. Gu, M. Huang, J. Liu, Y. Li, W. Zhao and J. Shi, Calcium doped mesoporous silica nanoparticles as efficient alendronate delivery vehicles, *New J. Chem.*, 2012, **36**, 1717–1720.

62 F.-C. Wu, R.-L. Tseng, S.-C. Huang and R.-S. Juang, Characteristics of pseudo-second-order kinetic model for liquid-phase adsorption: A mini-review, *Chem. Eng. J.*, 2009, **151**, 1–9.

63 G. Hong, L. Shen, M. Wang, Y. Yang, X. Wang, M. Zhu and B. S. Hsiao, Nanofibrous polydopamine complex membranes for adsorption of Lanthanum(III) ions, *Chem. Eng. J.*, 2014, **244**, 307–316.

64 J. P. Tang, M. Y. Huang, Z. X. Liang, Y. H. Wen, Q. L. Zhu and X. T. Wu, Water-Stable Two-Dimensional Metal–Organic Framework Nanostructures for Fe^{3+} Ions Detection, *Cryst. Growth Des.*, 2021, **21**, 5275–5282.

65 Z. J. Li, Z. Yue, Y. Ju, X. Wu, Y. Ren, S. Wang, Y. Li, Z. H. Zhang, X. Guo, J. Lin and J. Q. Wang, Ultrastable Thorium Metal-Organic Frameworks for Efficient Iodine Adsorption, *Inorg. Chem.*, 2020, **59**, 4435–4442.

66 G. Massasso, M. Rodriguez-Castillo, J. Long, A. Grandjean, B. Onida, Y. Guari, C. Guerin and J. Larionova, Nanocomposites based on Hofmann-type structure NiII(pz)[NiII(CN)4] (pz=pyrazine) nanoparticles for reversible iodine capture, *J. Mater. Chem. A*, 2015, **3**, 179–188.

67 X. Li, G. Chen and Q. Jia, One-pot synthesis of viologen-based hypercrosslinked polymers for efficient volatile iodine capture, *Microporous Mesoporous Mater.*, 2019, **279**, 186–192.

68 X. Guo, Y. Li, M. Zhang, K. Cao, Y. Tian, Y. Qi, S. Li, K. Li, X. Yu and L. Ma, Colyliform Crystalline 2D Covalent Organic Frameworks (COFs) with Quasi-3D Topologies for Rapid I_2 Adsorption, *Angew. Chem., Int. Ed.*, 2020, **59**, 22697–22705.

69 N. Liu, J. Chen, Z. Wu, P. Zhan, L. Zhang, Q. Wei, F. Wang and L. Shao, Construction of Microporous Lignin-Based Hypercross-Linked Polymers with High Surface Areas for Enhanced Iodine Capture, *ACS Appl. Polym. Mater.*, 2021, **3**, 2178–2188.

70 Q. Sun, B. Aguila, J. A. Perman, T. Butts, F.-S. Xiao and S. Ma, Integrating Superwettability within Covalent Organic Frameworks for Functional Coating, *Chem*, 2018, **4**, 1726–1739.